AD NUMBER
AD317281
CLASSIFICATION CHANGES
TO: unclassified
FROM: confidential
LIMITATION CHANGES
TO: Approved for public release, distribution unlimited
FROM: Controlling DoD Organization: Office of Naval Research, Arlington, VA 22203.
AUTHORITY
Office of Naval Research ltr dtd 28 Jul 1977; Office of Naval Research ltr dtd 28 Jul 1977

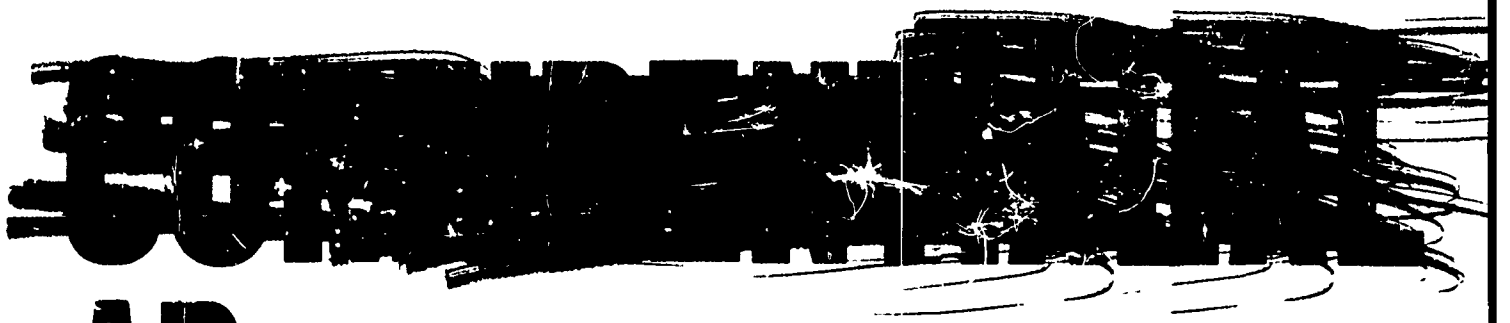

AD

317 281

MASSACHUSETTS INSTITUTE OF TECHNOLOGY
NAVAL SUPERSONIC LABORATORY

Wind Tunnel Report 376

(UNCLASSIFIED TITLE)

WIND TUNNEL TEST OF AN INFRARED WINDOW FOR AN/DAN-5 GUIDANCE SYSTEM

by

Lawrence D. Lorah

and

Raymond B. Tourtellot

March 1960

CONFIDENTIAL

Massachusetts Institute of Technology
Naval Supersonic Laboratory

Wind Tunnel Report 376

(UNCLASSIFIED TITLE)

WIND TUNNEL TEST OF AN INFRARED WINDOW FOR AN/DAN-5 GUIDANCE SYSTEM

by

Lawrence D. Lorah

and

Raymond B. Tourtellot

Contract No. Nonr 1841(40)
DSR 8150

March 1960

This document contains x
and 40 pages. Copy No. 9
of 75 copies.

NSL Log No. 3616

CONFIDENTIAL

FOREWORD

The experimental program discussed in this report is part of a larger project at the Naval Supersonic Laboratory supported jointly by the Navy's Bureaus of Aeronautics and Ordnance (now Bureau of Naval Weapons) and by the Office of Naval Research. This work was administrated through Contract Nonr 1841(40).

ABSTRACT

A wind tunnel program is discussed in which the AN/DAN-5 infrared guidance system, as installed in the Sparrow III missile, was equipped with a four-jet aerodynamic window. The tests were carried out at Mach numbers of 2.75 and 3.0 over a limited range of jet parameters. Internal pressure measurements were made from which the overall axial force and pressure loading of the missile shell can be estimated. Noise level measurements were made inside the missile. In addition, the aerodynamically produced torques on the guidance system telescope were also measured. Conclusions pertinent to a captive flight test of this configuration are drawn from the data.

TABLE OF CONTENTS

LIST OF ILLUSTRATIONS

LIST OF ILLUSTRATIONS Concluded

LIST OF TABLES

LIST OF SYMBOLS

A^*_j	Total jet throat area
A_m	Model face area
A_E	Nozzle exit area
B	Angle between jet nozzle axis and model face
C_x	Nose axial force coefficient, F_x/qA_m
C_τ	Torque coefficient, τ/qD^3
D	Model diameter
F	Force
I	Moment of inertia of telescope
JFR	Jet flow ratio
K	Hydraulic pressure to torque conversion factor
$\dot{m}$	Mass flow
M	Mach number
P	Static pressure
P_0	Stagnation pressure
q	Dynamic pressure (free stream)
T	Static temperature
T_0	Stagnation temperature
v	Velocity
W	Weight of telescope
x	Distance from telescope c.g. to axis of rotation
γ	Ratio of specific heats of air
ϕ	Telescope position with respect to pressure taps
θ	Telescope deflection

LIST OF SYMBOLS Concluded

$\ddot{\theta}$	Angular acceleration
τ	Torque

Subscripts

e.p.	Due to jet exit pressure
f	Face, or due to face pressure
j	Jet
jmc	Due to jet momentum change
M	Evaluated at Mach number M
T or t	Tunnel (free stream)

I. INTRODUCTION

It has long been recognized that infrared guided missiles are severely affected by aerodynamic heating at supersonic speeds. The major difficulty arises when the infrared transmitting window, usually the nose of the missile, becomes hot and subsequently loses its infrared transparency. At the same time it begins to radiate enough energy to saturate the sensitive element. Both of these effects cause a severe loss in system sensitivity and thus a severe decrease in maximum detection range for a given target. Within 10 to 20 seconds of flight at moderate Mach numbers and altitudes the hot window effects render conventional systems nearly useless.

A promising solution to the hot window problem has been proposed by the Naval Supersonic Laboratory (NSL) in which the radiating, non-transmitting physical window is replaced by an aerodynamic shield. In one possible configuration, four supersonic jets of air, equally spaced around the periphery of the missile face, are directed into the free stream. These jets converge a short distance ahead of the missile and produce a nearly conical shock wave in the main flow. Experimentally, it has been found that this flow configuration results in low pressures and reduced heat transfer rates on the face of the missile – in short, it results in an environment at the missile face in which an unprotected infrared tracking system could operate. Details of the effects of the hot window problem on infrared guidance, and discussion and description of several aerodynamic window configurations tested by the Naval Supersonic Laboratory in its wind tunnel are contained in Ref. 1.

In order to establish more firmly the feasibility of using the NSL aerodynamic window in free flight, it has been proposed to run a captive flight test utilizing a current infrared system. In the proposed experiment the infrared guidance system, in the missile configuration, would be operated with an aerodynamic window while being carried by a supersonic aircraft. The wind tunnel programs discussed in this report were intended to fix aerospike design parameters (jet nozzle design and optimum jet flow ratio) and measure some of the aerodynamic loads

likely to be encountered in the flight test without the usual physical window. The infrared system which is considered is the AN/DAN-5 as installed in the infrared version of the Sparrow III missile. The tentative flight conditions are about Mach 2.0 at 30,000 ft. to 40,000 ft.

II. EXPERIMENTAL EQUIPMENT

A. Wind Tunnel

The experiments were carried out in the Naval Supersonic Wind Tunnel. The basic tunnel can produce flow velocities ranging from subsonic to Mach 4.0 at stagnation pressures from about 0.5 psia to about 40 psia. At supersonic Mach numbers up to 2.5 and at Mach 4.0 the test section is 18 by 24 inches. At other supersonic Mach numbers the test section is 18 by 18 inches. A detailed description of the wind tunnel will be found in Ref. 2.

Since it was decided to operate the full scale infrared equipment in the wind tunnel, flow blockage was an important test consideration. A short series of tests was run in the tunnel to determine the lowest Mach number at which an eight inch diameter, blunt faced model could be run without blocking the flow (blocking is less of a problem at higher Mach numbers, generally). It was found that, with a modified installation, the wind tunnel would run at a Mach number of 2.75 or above with the proposed model. This fixed a lower Mach number limit for the remainder of the program.

B. Infrared System

The infrared guidance system used in the experiment was the AN/DAN-5 as mounted for use in the Sparrow III air-to-air missile. The missile outside diameter was eight inches, and normally the tracking gear is housed behind an eight inch diameter quartz hemisphere. This hemisphere was removed for operation with the aerodynamic window, exposing the forward cavity of the guidance system. This section contained the tracking telescope mounted on hydraulically driven gimbals along with the rate sensing gyros. Figure 1 shows, schematically, the general layout of the telescope and gimbal system within the cavity. Notice should

be taken of the hydraulic activators (the piston-cylinder assemblies) which drive the telescope in pitch and yaw. A full description of the operation of the tracking system can be found in Ref. 3.

The infrared detecting portion of the system was not used in this wind tunnel program. Continuous hydraulic power was supplied by a pump outside the wind tunnel, and this closed circuit system allowed the head to be moved throughout the wind tunnel tests. In place of the error signal from the infrared detector, commands were fed into the head positioning servo from a control panel outside the wind tunnel. A large variety of head movements were available; not only through a continuous range of pitch and yaw positions, but also a variety of time histories (step command, ramp command, sinusoidal oscillations, etc.). Potentiometers on the axes of rotation were monitored to give true head position at any time.

C. Aerodynamic Window

The four-jet aerodynamic spike configuration was chosen because of the physical space limitations within the head. The single-jet configuration was discarded for this particular test due to the unknown effects of optical blocking of the primary mirror by the jet producing equipment. It was felt that all the plumbing for the jets should be contained within the basic eight inch shell. Because of the gimbal arm and gyro clearance there were only four relatively small "channels" through which jet air could be brought to the missile face. A manifold at the missile face, feeding any number of jets, would have to have been forward of the telescope (for clearance reasons) and therefore would have tended to block the telescope field. The jet air supply was brought to two manifolds near the back of the gimbal assembly, then was fed through four ducts to the jets. Each of the four ducts was composed of three pipes because of strength and space considerations. Figure 2 shows, again schematically, the layout of the jet system.

The basic structural member in the assembly was the gimbal ring, shown in the figure. The infrared system and the jet equipment were both mounted on this piece. There was a need for a covering shroud to extend from the ring forward to the vicinity of the jet exit. The length of this

shroud was varied, so that its face was approximately even with the jet exit plane, 1-7/8 inches behind the jet exit plane, and 3-3/4 inches behind the jet exit plane.

The supersonic jets were formed as the high pressure air was expanded through the nozzles shown in Fig. 2. The nozzles were made so that they might be changed to vary the jet parameters. The nozzle throat diameters took on two values, 0.253 inches and 0.179 inches. The exit areas of the nozzles were selected to give jet Mach numbers of 3.0 and 4.0 for each throat diameter. Thus, there was a total of four sets of jet parameters available. As shown in Fig. 2, the jet nozzles were equally spaced around the periphery of the model, and the nozzle axes converged at an angle of 27° with respect to the model axis. Figure 3 is a photograph of the completed model installed in the wind tunnel.

D. Instrumentation

The following is a brief description of the instrumentation used throughout the program. The tests were run in two phases and not all the instrumentation was used in both phases.

1. Free Stream Parameters

The free stream Mach number was fixed by wind tunnel geometry, and so, remains constant throughout at 2.75. Stagnation temperature and pressure were measured by the standard thermocouples and pressure taps in the tunnel and were hand recorded from the console instruments. Schlieren photographs were also taken.

2. Jet Parameters

In addition to the jet Mach number, which was determined by the nozzle geometry, the jet stagnation pressure and temperature were measured to compute the jet performance parameter, JFR, (see Appendix A). The stagnation temperature was measured by means of a thermocouple projecting into the jet flow just before it entered the contracting section of one of the jet nozzles. The jet temperature was automatically recorded on a Bristol strip chart. The stagnation pressure

was measured at a similar point in another nozzle feed line, and was hand recorded. It was assumed that the temperature and pressures in all four nozzles were the same.

3. Internal Model Pressures

Four static pressure taps were placed on the inside of the shroud to measure the pressure adjacent to the telescope. The taps are equally spaced around the shroud, 45° from the jet nozzles, approximately in the plane containing the axes of rotation of the telescope. The pressure within the missile was measured by four pressure taps placed behind the gimbal ring, near the yaw actuator. These probes indicated the internal pressure loading due to the scoop effect of the open missile face. In addition, it has been determined (Ref. 4) that the pressure is fairly uniform over the face of a model such as this when the jets are off, or when they are operating near the minimum drag condition. Therefore this internal pressure measurement also gives a good indication of the pressure drag of the total configuration under the conditions of interest in this report.

4. Internal Noise Measurement

Because of the open cavity in supersonic flow, there is a possibility of intense noise within the missile. To monitor the noise, a crystal microphone (Massa Lab. Inc., Model M -141b) was mounted aft of the gimbal ring in an area considered to be free of "gusts" and "drafts" along the centerline of the missile. The rms microphone output was read on a VTVM. The data is presented as an rms oscillation in the static pressure level measured in lbs/in.^{2}

5. Telescope Torque

One of the prime pieces of information desired in the second phase of the program was the aerodynamically produced torque applied to the telescope. In order to facilitate positioning the missile telescope when it was in the wind tunnel, and to allow torque measurements to be made while the head was moving, it was decided to infer torque loading from hydraulic pressure measurements. A manifold was installed at the servo-driven hydraulic valves so that the pressures in the four actuator cylinders (two in pitch and two in yaw) could be measured. The pressure difference in a pair of cylinders is related to the torque loading on the

telescope through the gimbal and actuator geometry (see Fig. 4). Pressure transducers with a range of 0-2000 psia were used to measure the hydraulic pressures up to 1700 psia. The outputs of the pressure transducers were fed into a recording oscillograph so that the torque could be computed for conditions when the head was moving as well as stationary.

A block diagram of the instrumentation is shown in Fig. 5.

III. EXPERIMENTAL PROCEDURE AND RESULTS

A. Test Phase 1

Apart from the blocking tests already mentioned, the experiment was divided into two phases. The first phase was intended to determine the best set of jet parameters and shroud length with respect to overall drag and internal pressure fluctuations. From previous work at NSL the ranges of jet parameters (jet Mach number and A^*_j/A_m) for minimum nose axial force were narrowed considerably (Ref. 1). The limits on shroud length were fixed by practical considerations - it must be short enough to allow the telescope to have a reasonable field of view and long enough to establish a "face" on which aerodynamic window phenomenom could build.

Throughout the first phase, the following parameters were held at the values noted:

tunnel Mach number	2.75	roll angle	0°
angle of attack	0°	$T_{0_T}/T_{0_j} \approx 1$	

During the wind tunnel experiment the jet parameters and shroud length were selected and then a tunnel stagnation pressure was set. At these conditions the jet pressure was varied to get nose axial force and internal noise as a function of jet flow ratio as it varied from no flow to beyond the minimum axial force condition. The condensed run schedule for this test phase is shown in Table I.

Typical schlieren photographs are shown in Fig. 6. It can be seen that the free stream flow was smooth and steady with no flow through the jets and that there was a near normal shock wave standing a short distance from the missile face. In the second photograph the formation of the aerodynamic window is shown. The curved shock wave in the main stream developed as the jet strength became adequate with the resulting

TABLE I

Condensed Run Schedule, Test Phase 1

Run no.	M_j	A_j^*/A_m	P_{0_T} (psia)	Shroud Length (in)	P_{0_j} (psia)
1	3.0	0.002	3.0	6-7/8	0-50 (typical)
2	4.0	0.002	3.0		
3	3.0	0.004	6.0		
3A	3.0	0.004	3.0		
3B	3.0	0.004	4.0		
4	4.0	0.004	3.0		
5	3.0	0.004	3.0	5	
6	3.0	0.004	3.0	8-3/4	0-50 (typical)

reduction in pressure across the missile face. These pictures indicate that the flow over this open model was essentially the same as that observed over flat faced models tested in the past.

The drag measurements made in the program are probably not quite as accurate as those previously obtained. However, they certainly are precise enough to allow the type of comparisons between configurations needed here. The data is presented in the form of nose axial force coefficient as a function of jet flow ratio. (see Appendix A for definitions). The first thing that must be established is the validity of this type of non-dimensionalization. It is already known that C_x as a function of JFR changes somewhat with free stream Mach number. In fact, it was shown in Ref. 1 that the minimum nose axial force coefficient of the multiple jet aerodynamic spike configuration varies as the drag coefficient of a 30° half angle cone over a Mach number range of at least 2.0 to 3.5. Figure 7 shows C_x vs. JFR for a given model configuration at several values of wind tunnel stagnation pressure. This figure shows that, at least in the drag region of interest, the C_x variation with JFR is independent of free stream pressure level. Thus, if the Mach number correction mentioned above is made, the C_x and JFR non-dimensionalizations are valid ones over the present range of interest.

In Fig. 8 the four sets of jet parameters are compared in overall axial force performance. It appears that there is very little variation in the C_x dependence on JFR. The usual vagaries show up at the break point (i.e. the region where C_x drops very rapidly to near its minimum value), but, within the experimental accuracy, a single line can be drawn through all the points in the critical minimum C_x region. These results are in agreement with the findings of Ref. 4. Therefore, the jet parameters of Mach number and ratio A^*_j / A_m can be chosen (within the limits of the experiment) to simplify operational problems of jet gas supply.

The changes in C_x with changing shroud length were equally unexciting. Nose axial force coefficients measured with the medium and short shrouds are shown in Fig. 9. Again the improvement of one configuration over the other was not large enough to be significant. An attempt to measure C_x with the long shroud was hampered by intermittent tunnel blockage, and this data is not shown in Fig. 9 because it is considered somewhat unreliable. If anything, C_x increased slightly with the installation of the long shroud.

The pressure fluctuations within the open missile are of importance if they are very strong. Acoustic vibrations can cause microphonic noise in the electronic components and even structural damage under some conditions. The configuration under study, an open-ended cylinder behind an unsteady shock structure, suggests very high noise levels in the missile interior, and it was deemed necessary to measure the noise levels within the cavity. As mentioned previously, the measurements were made with a microphone mounted behind the gimbal ring.

The acoustic data is presented as the ratio of the root mean square pressure fluctuation divided by the stagnation pressure of the free stream. Figure 10 shows the measurements taken at three free stream pressure levels for a given configuration, as a function of jet flow ratio. The pressure fluctuation, non-dimensionalized by P_{0_T}, is shown in the figure to be independent of pressure level. The acoustic noise shows a rather interesting behavior as a function of jet flow ratio. The noise level was comparatively low when the jets were off and a steady shock wave was formed ahead of the body. The level of pressure fluctuation increased rapidly to a maximum value, nearly an order of magnitude greater, at

a jet flow ratio slightly less than that for minimum drag. It then fell off and approached a constant value in the overblown condition. At the minimum drag point the noise level was about a factor of two less than the maximum value. For low values of jet flow ratio, i.e., when the jets were just beginning to form, there was a great deal of scatter in the data just as there usually is in the axial force measurements due to the unsteadiness and non-repeatability of the flow conditions. Fortunately this is not the area of interest since it does not correspond to desired operating conditions and does not represent a maximum between the two operating conditions (JFR and minimum C_x).

The internal noise present in the various configurations is compared in Fig. 11. As was expected from the results of C_x measurement, there was no significant, consistent difference in noise level among the configurations near the region of interest. The short shroud produced slightly less noise at high jet flow ratios.

It was suggested in Ref. 5 that the noise levels behind a shock system similar to the one under study was proportional to the free stream dynamic pressure, q. This allows the results of Fig. 11 to be adjusted to a Mach number other than 2.75.

B. Test Phase 2

During the second phase of testing, the model configuration was held constant. The tunnel pressure was varied and the tunnel Mach number took on two values to facilitate determining the variation of torque on the telescope with Mach number. The fixed parameters were

Angle of Attack	0°
Roll angle	0°
M_j	3.0
A^*_j/A_m	0.004
T_{0_T}/T_{0_j}	$\approx$ 1
Shroud length	medium

At each set of tunnel conditions data was taken with the jets off and with a jet flow ratio of 0.1 (i.e., a JFR slightly above that needed for minimum drag.) A condensed run schedule for the second phase of the

program is shown in Table II.

TABLE II

Condensed Run Schedule, Test Phase 2

Run no.	M_T	P_{0_T}(psia)
1	2.75	11.5
2	2.75	25
3	3.00	25
4	3.00	15

The measured shroud pressures are shown in Fig. 12 as a function of head position. The variable, ϕ, denotes the head position; zero ϕ indicates an on-axis position with a positive ϕ indicating head movement away from the pressure tap under consideration, and minus ϕ indicating movement toward the pressure tap under consideration. The variation of pressure with head position was probably due to the fact that there was some flow through the missile (the model not being completely sealed at the aft end). It was accelerated locally to some extent, depending on the open area near the pressure taps. This open area, of course, changed as the telescope was moved. The measured pressures were a little below the pressure expected for a completely sealed missile. This pressure is shown as the line $C_{x_f} q / P_{0_T}$. The minimum possible pressure outside the shroud is the static pressure in the free stream. The actual static pressure is somewhat higher because of the obliquity of the shock wave. However, an estimate of the pressure loading on the shroud and missile skin with the jets in operation, can be obtained by taking the difference between the measured internal pressures and static pressure behind a normal shock. To obtain a similar estimation of this pressure loading, for a jet flow ratio of zero, the difference between stagnation and static pressure behind a normal shock in the free stream can be taken. The pressure difference across the missile skin is greatest at a jet flow ratio of zero.

Additional internal sound measurements were made during the second phase of the test program. Once the approximate level of the pressure fluctuations had been established, the variation with head position was determined. Plots of constant values of rms $\Delta P / P_{0_T}$ over the entire range of pitch and yaw positions are shown in Fig. 13. This second set of measurements shows a slight variation in sound level for the telescope at the on-axis position (about a 40 percent deviation). However, this probably can be attributed to modifications in the model installation and changes in the operation of the wind tunnel equipment. It can be seen that the variation in fluctuating pressure level was small with variations in head position, amounting to about 10 percent of the overall level. The asymmetry in Fig. 13 is due to the asymmetry of the telescope and gimbal mounting.

The prime purpose of the second test phase was the measurement of the additional torque loading on the tracking telescope due to the removal of the protective, quartz dome. Structurally, the telescope and gimbal system can withstand the forces aerodynamically applied to them. However, there exists the possibility that the aerodynamic torques can overpower the hydraulic activating system.

Measurement of torque loading on the telescope was plagued with difficulties. As previously discussed, the torque was determined by measuring the pressure difference between the two activator cylinders for each plane. During the bench tests prior to the wind tunnel program it was apparent that the torque measurements taken when the head was stationary were non-repeatable and generally unreliable. This was attributed to such practical difficulties as friction caused hysteresis seal and valve non-uniformities, and electronic "dither" superimposed on the valve motion. Discussion with the manufacturers of the equipment revealed that this behavior is common and not due to malfunction of the particular system under test. It was discovered that repeatable data of less dubious quality could be taken while the head was in motion. This means that the inertial and friction loads as well as the head weight must be considered when reducing the torque data. It can be seen that the usual dynamic torque equation may be written,

$$I_1 \ddot{\theta} = \tau_{\text{hydraulic}} + \tau_{\text{aerodynamic}} + \tau_{\text{friction}} + \tau_{\text{gravity}}$$

The hydraulic torque is that applied by the activators. The term representing the torque due to friction is dependent on the angular velocity, both magnitude and direction. The torque due to gravity comes about because the head center of gravity is displaced from the center of rotation; this must be considered only in the pitch plane. The aerodynamic torque is the desired quantity. If the telescope is driven at a constant angular velocity, the equation can be written

$$\tau_{aerodynamic} = - \Delta P_{hyd} K - Wx - \tau_{friction}.$$

By applying known torques in place of $\tau_{aerodynamic}$, the values of $\tau_{friction}$ were found for the ranges of angular velocity and position of interest.

The procedure followed in obtaining the torque data was to set the head at various pitch angles and drive it back and forth through the yaw range to measure aerodynamic torque in the yaw direction. The process was repeated in the other direction to obtain torque data in the pitch direction. Two wind tunnel pressures at each of two Mach numbers were investigated (see Table II) with the jets turned off and with the jets operating at a jet flow ratio of 0.1.

Samples of the torque data are shown in Figs. 14 through 21. In these figures the torque in the pitch direction is plotted against pitch angle for various values of yaw as the head was driven in the pitch plane. The yaw torque data is presented similarly. Data for only three angular positions about the axis of motion was reduced; the data for some angles perpendicular to the axis of motion was omitted for clarity. The torque data obtained in this phase of the program proved rather erratic. This is probably due to the fact that the aerodynamic torque levels experienced in the wind tunnel were on the order of 5 percent of the system capability. Even though the errors due to friction, etc., were reduced by taking the data while the telescope was moving, they could not be eliminated entirely. Thus the scatter in the data was not too suprising. In spite of the seeming chaos in the curves, several things can be observed. Of significance is the fact that, generally, there appears to be little difference in the torque levels, for a given configuration, when the jets are off and when they are

operating near the minimum drag jet flow ratio. It is not clear how this observation can be justified in view of the fact that the face pressure level decreases when the jets are operated. Differences in C_τ were measured as a function of telescope position. These differences were not consistent from condition to condition and no overall trend can be found. Attempts to correlate C_τ with changes in Mach number proved fruitless. About all that can be said is that there is not a large change in average C_τ between Mach numbers of 2.75 and 3.00.

This uncertainty does not help the understanding of the phenomenon observed behind this type of aerodynamic window, but it does not preclude a favorable observation concerning the proposed flight test. By examining the figures it can be seen that only in one case ($M = 3.00$, $P_{\phi_T} = 15$) does the value of C_τ exceed 10^{-2} in either plane. Assuming that 10^{-2} represents the maximum C_τ experienced at a Mach number of 2.0, the maximum torque can be computed for sea level flight – it turns out to be about 186 in-lb. Now, the system under consideration is designed to operate at hydraulic pressures up to 2000 psia, and Fig. 4 shows that the minimum torque available at a telescope deflection of 40° is 216 in.-lb in pitch and 344 in.-lb in yaw. The hydraulic system then can handle the aerodynamic torque applied during Mach 2 flight at sea level even at an adverse telescope position. At high altitude, the dynamic pressure is down due to a decrease in static pressure and at low altitude Mach 2 flight is not practical and the dynamic pressure is again lower than for the above calculation. Thus under actual flight conditions the aerodynamic torque is much smaller than the torque capable of being applied by the hydraulic system.

IV. CONCLUSIONS

The following conclusions can be drawn from the test results discussed in the previous section. All discussion is for zero angle of attack, for air as a jet gas, and for conditions within the range of those tested.

1. The variation of C_x as a function of JFR is independent of free stream pressure level, at a given Mach number.

2. Within the range of jet parameters and shroud lengths tested, there is no significant change in the C_x variation with JFR. The

curve which holds for all configurations is shown in Fig. 8.

3. The variation of the rms internal pressure fluctuations, divided by the free stream stagnation pressure, as a function of JFR, is independent of the free stream pressure level at a given Mach number.

4. Within the range of jet parameter tested there is no significant change in the variation of $\Delta P / P_{0_T}$ as a function of JFR. The short-shroud configuration is slightly less noisy than the medium-shroud configuration at high JFR's (see Fig. 11).

5. The change in internal noise as the telescope position changes amounts to only about 10 percent of the overall rms noise level.

6. The maximum telescope torque coefficient, C_T, within the range of Mach numbers and pressures tested is 10^{-2} in both planes of movement. (one exception noted in discussion)

By applying the above results to the exact flight test conditions, once they are determined with some certainty, the expected levels of telescope torque, pressure loading of the shroud, and internal noise in the test missile can be estimated. In addition, the allowable levels of these quantities must be determined for the test configuration and compared to the estimated values.

REFERENCES

1. Fahrenholz, Fred E., Lorah, Lawrence D., Rubin, Eugene S., A Solution to the Hot Window Problem for Infrared Systems, Technical Report 415, Naval Supersonic Laboratory, Massachusetts Institute of Technology, September 1959. Confidential

2. General Information Bulletin, Naval Supersonic Laboratory, Massachusetts Institute of Technology, January 1959.

3. Handbook for Homing Set, Infrared AN/DAN-5 (XN-1), Bureau of Aeronautics, U.S. Navy, 1956. Confidential

4. Lorah, Lawrence D. An Experimental Study of a Window for an Infrared Seeker, WTR 276, Naval Supersonic Laboratory, Massachusetts Institute of Technology, January 1958. Confidential

5. Rubin, Eugene S. The Influence of Aerodynamic Heating on Infrared Systems, Technical Report 90, Naval Supersonic Laboratory, Massachusetts Institute of Technology, March 1956. Confidential

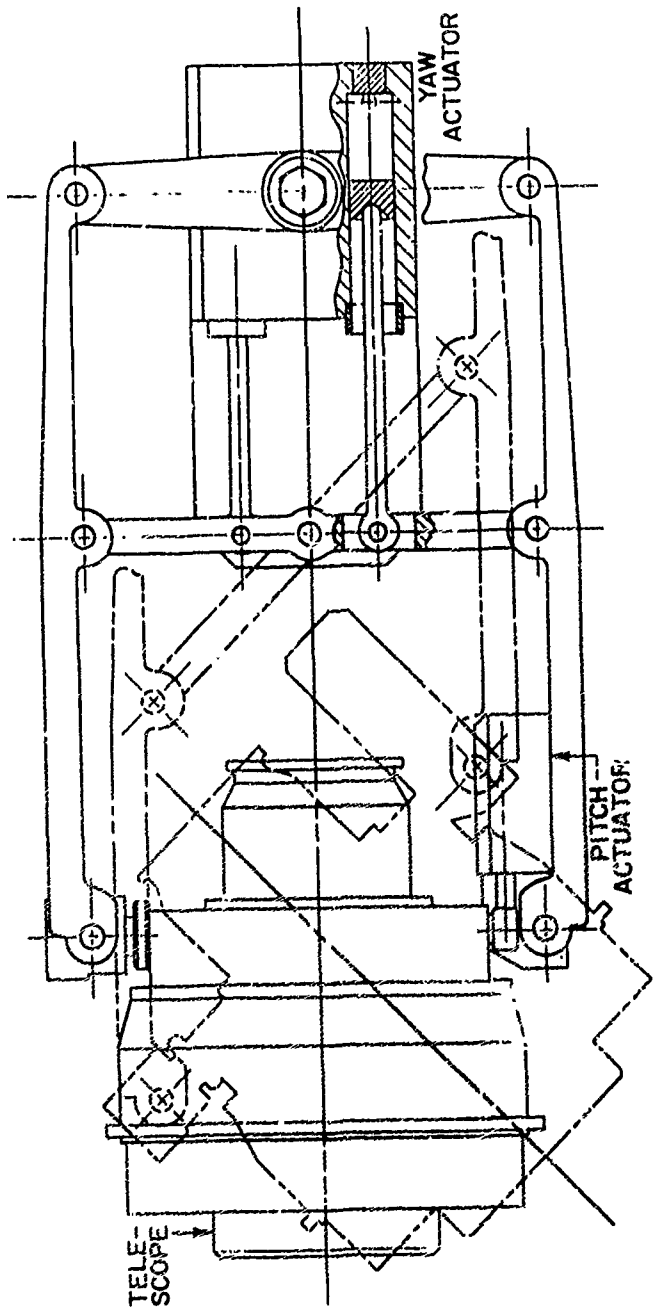

Figure 1a. Schematic Drawing of Tracking Telescope and Gimbal System, (Yaw Plane)

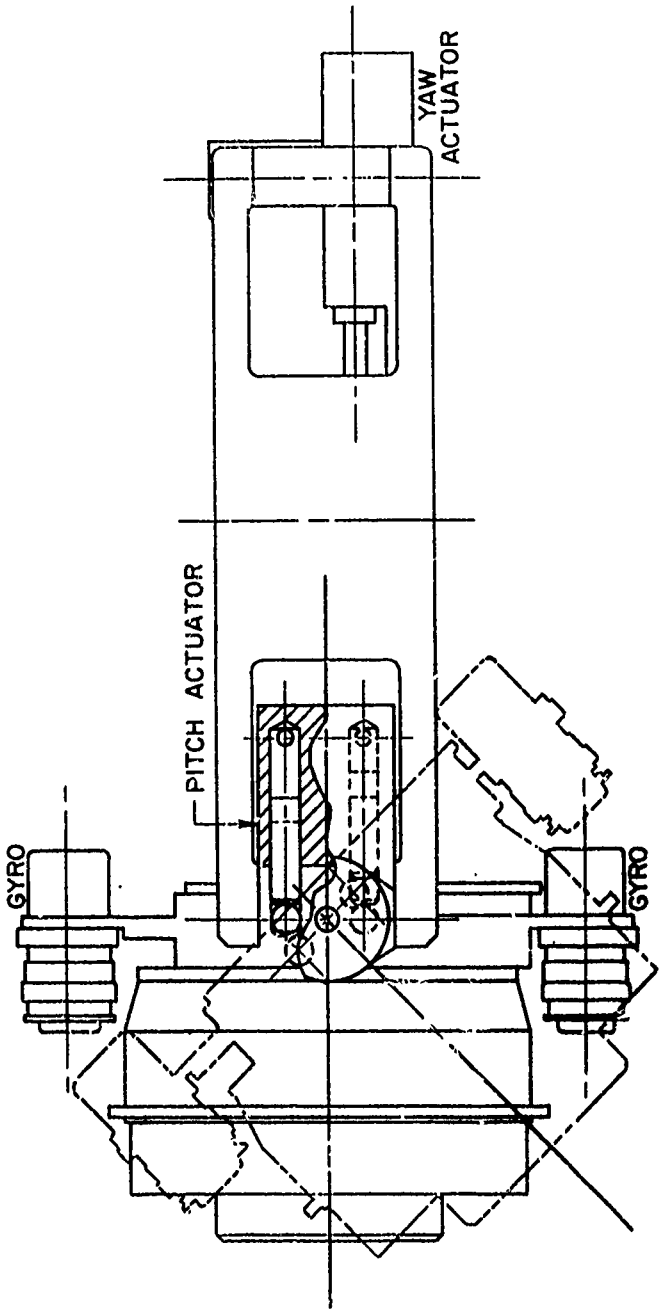

Figure 1b. Schematic Drawing of Tracking Telescope and Gimbal System, (Pitch Plane)

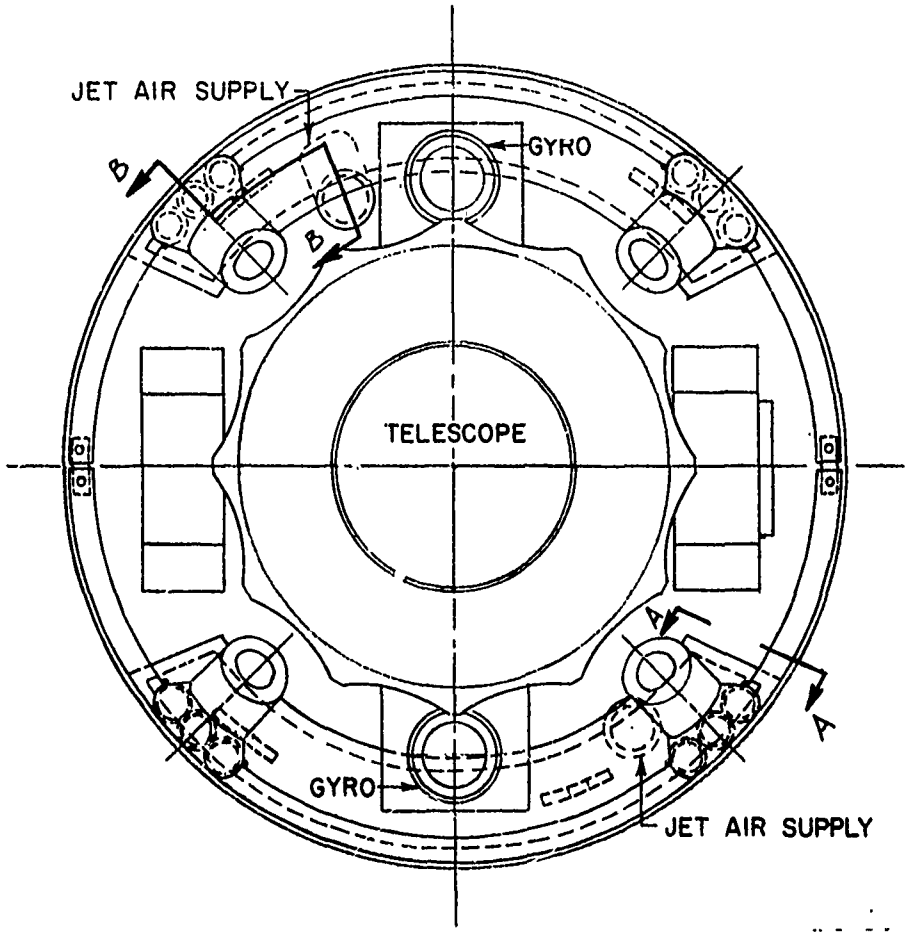

Figure 2a. Drawing of Jet Installation in Wind Tunnel Model (Front)

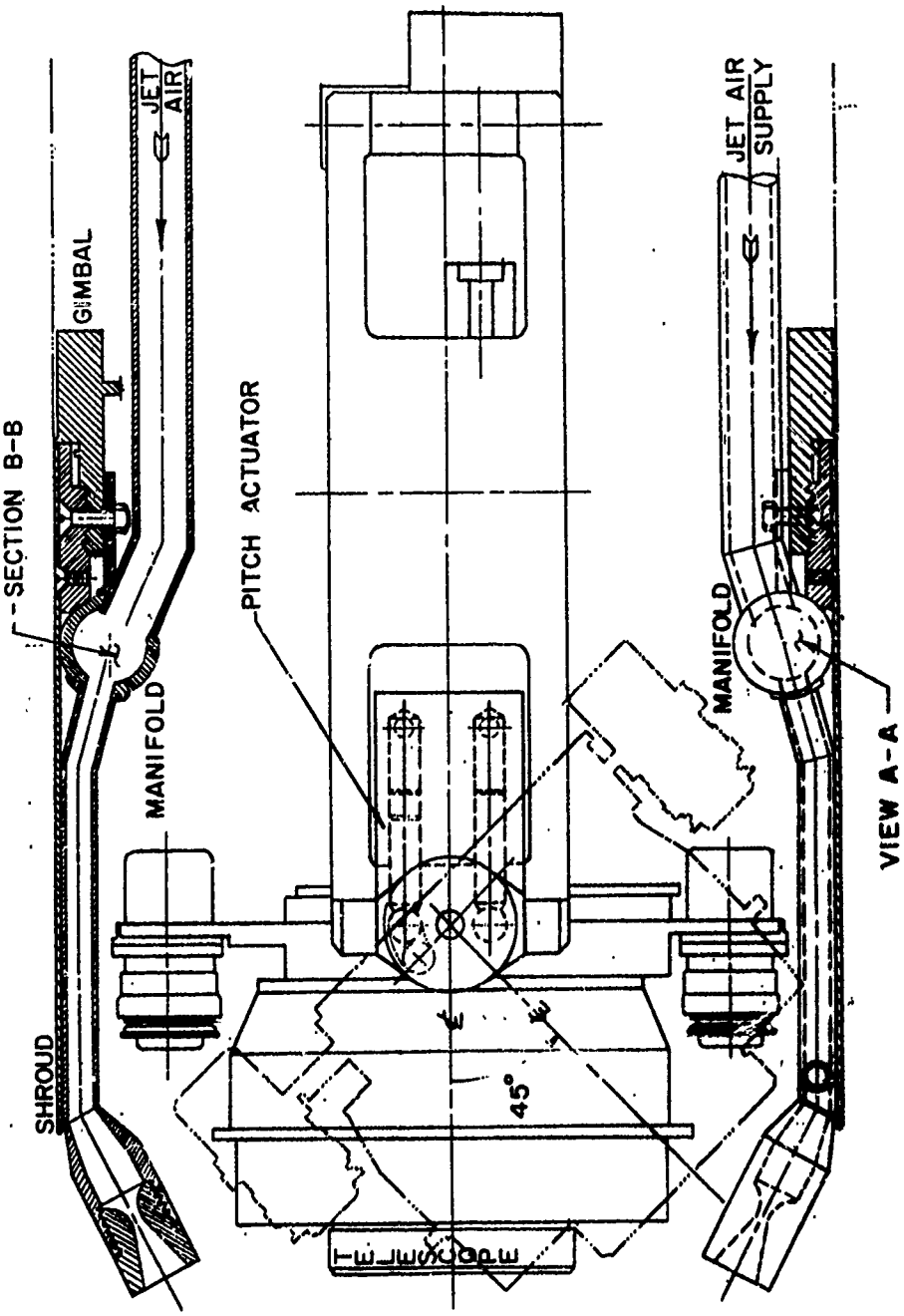

Figure 2b. Drawing of Jet Installation in Wind Tunnel Model (Side)

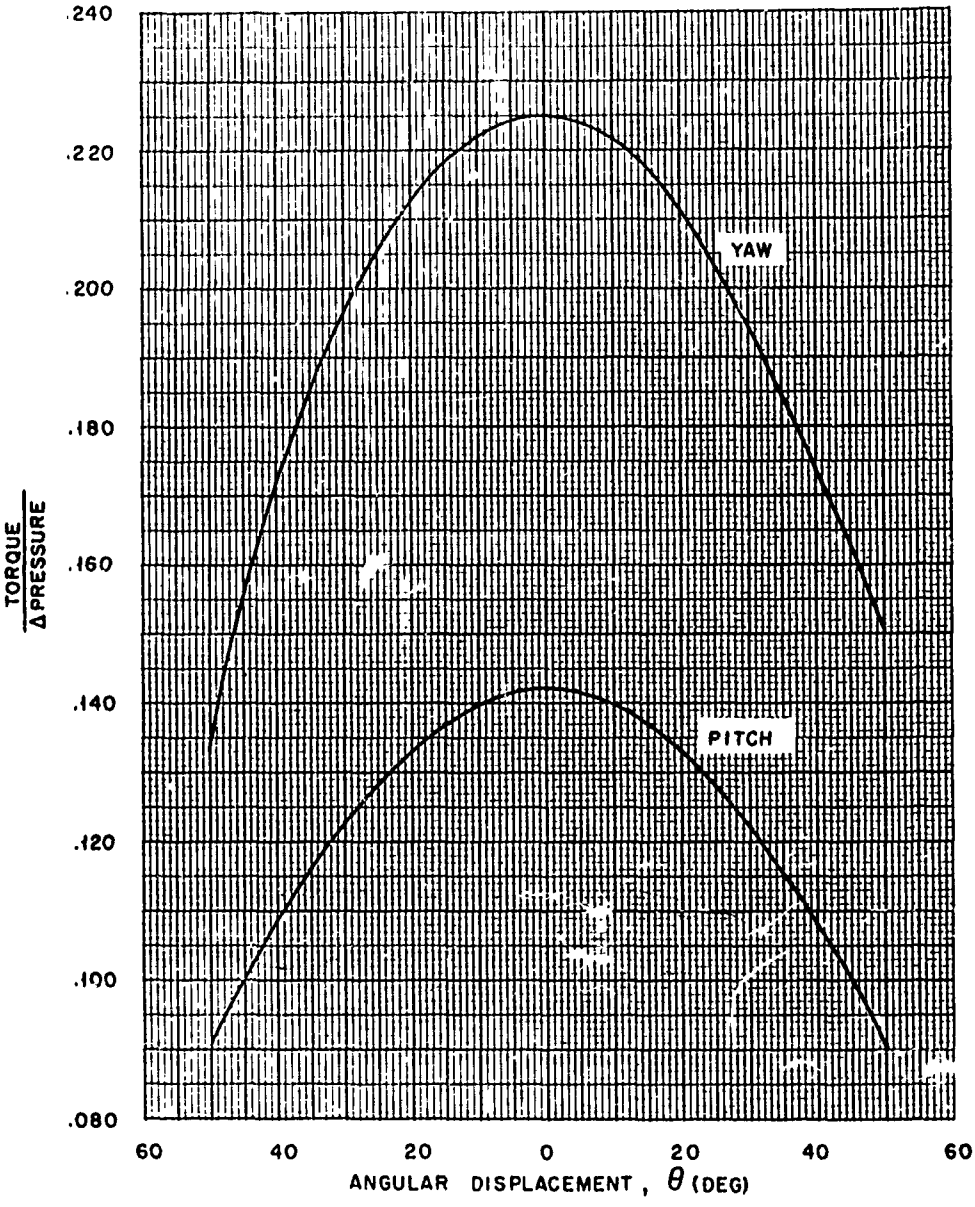

Figure 4. Torque on Telescope, Per Unit Hydraulic Pressure Differential as a Function of Telescope Deflection

JFR = 0

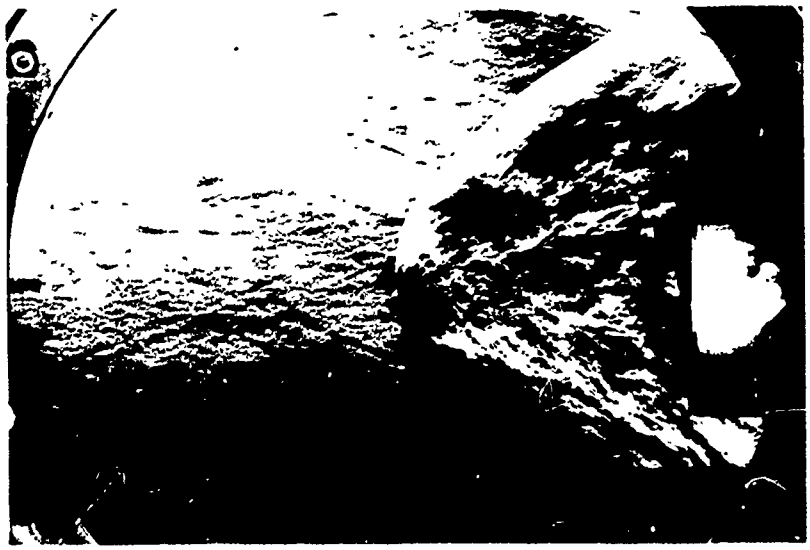

JFR = 0.10

Figure 6. Typical Schlieren Photographs of Aerodynamic Window Operation, M = 2.75

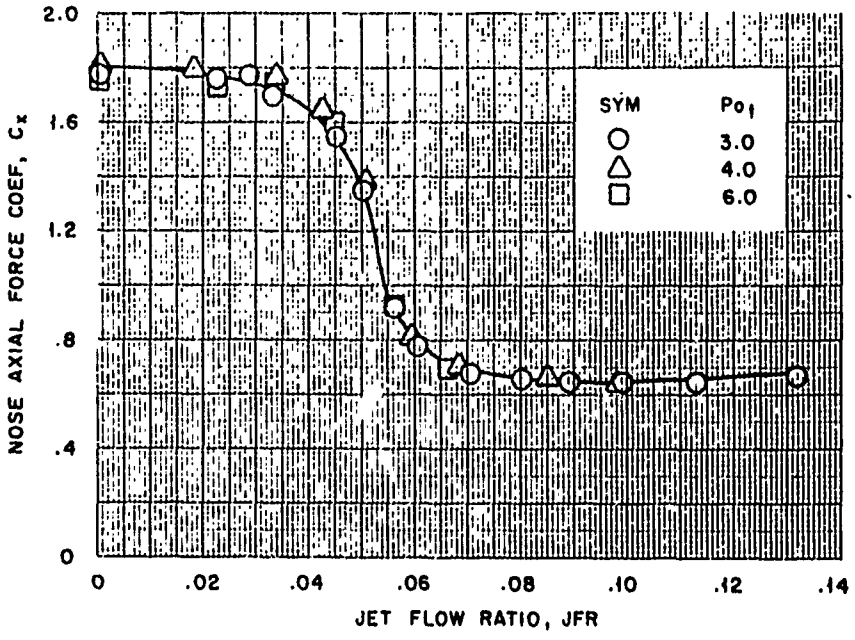

Figure 7. Nose Axial Force Coefficient vs. Jet Flow Ratio, Tunnel Pressure Variation

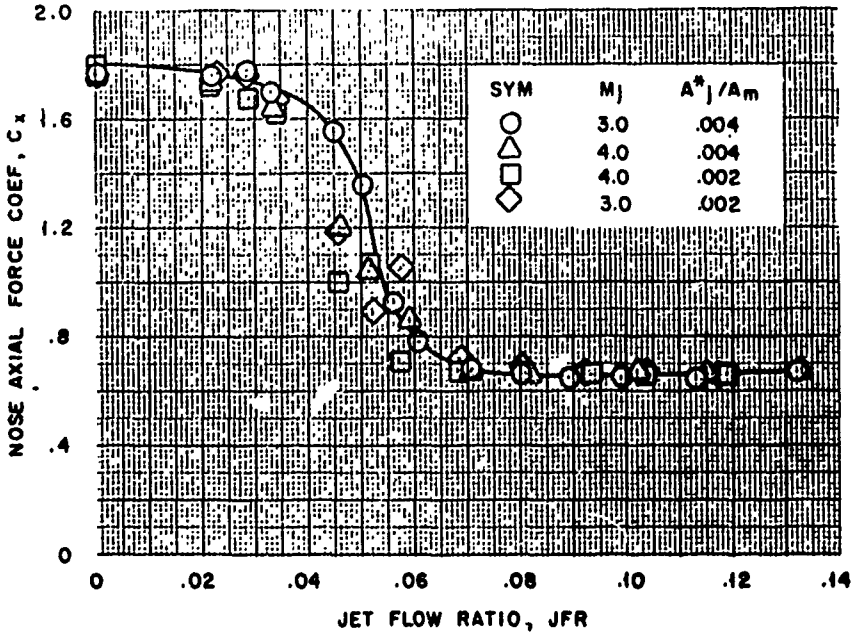

Figure 8. Nose Axial Force Coefficient vs. Jet Flow Ratio, Jet Parameter Variation

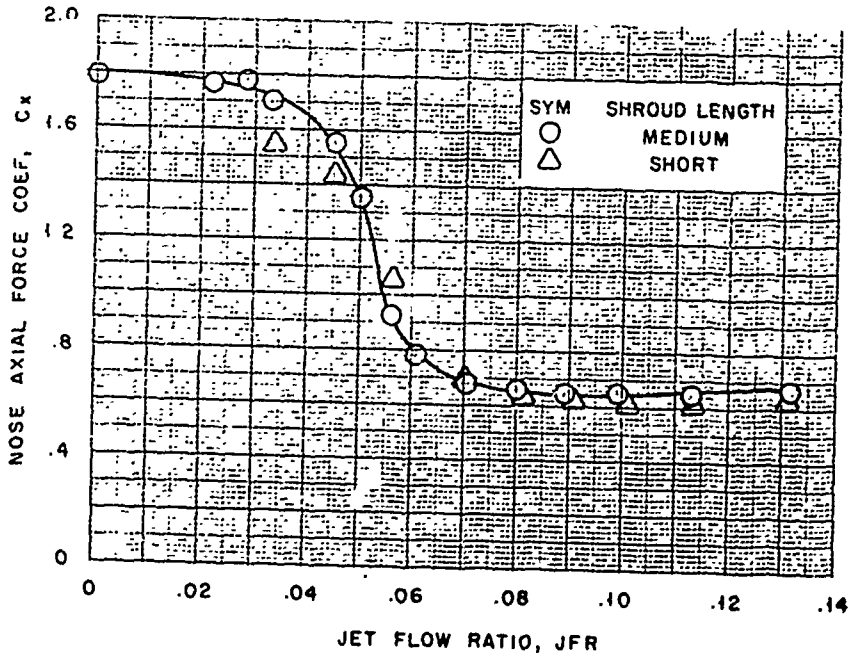

Figure 9. Nose Axial Force Coefficient vs. Jet Flow Ratio, Shroud Length Variation

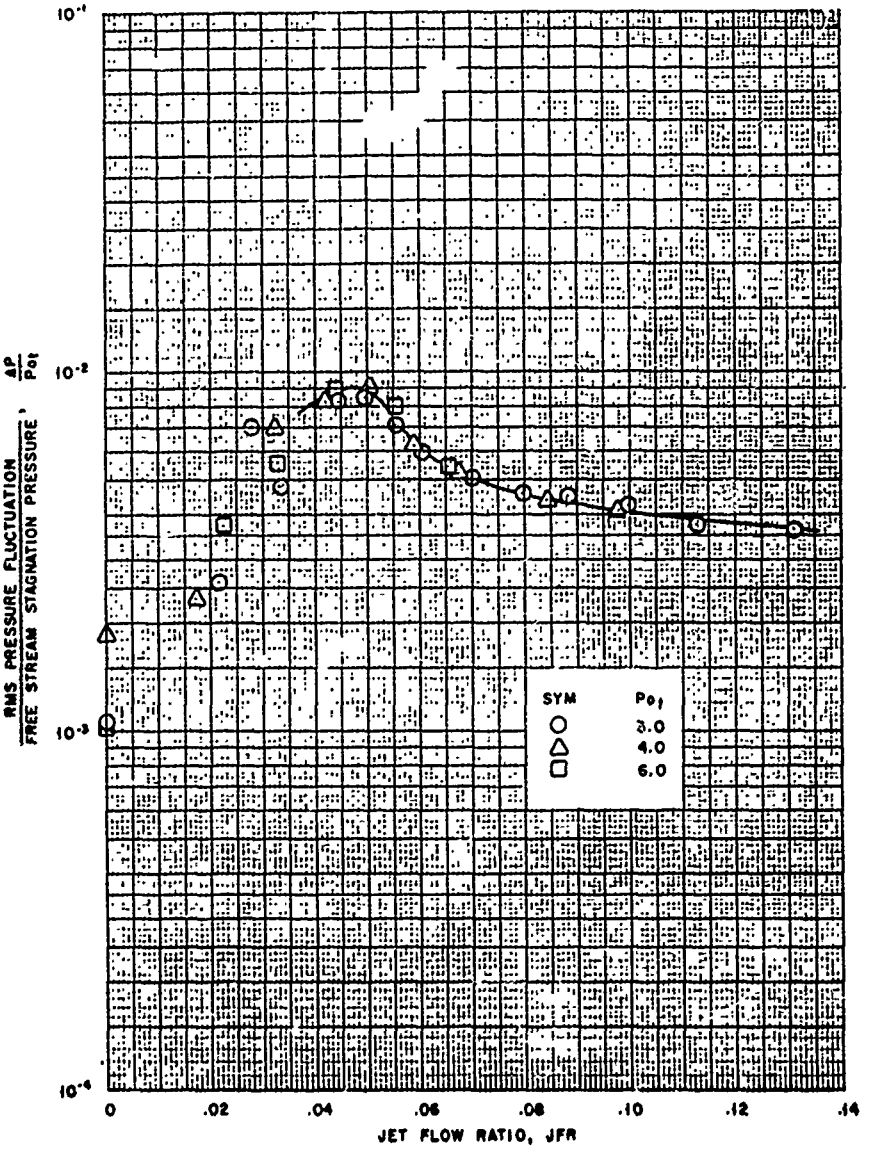

Figure 10. Root Mean Square Internal Pressure Fluctuations vs. Jet Flow Ratio, Tunnel Pressure Variation

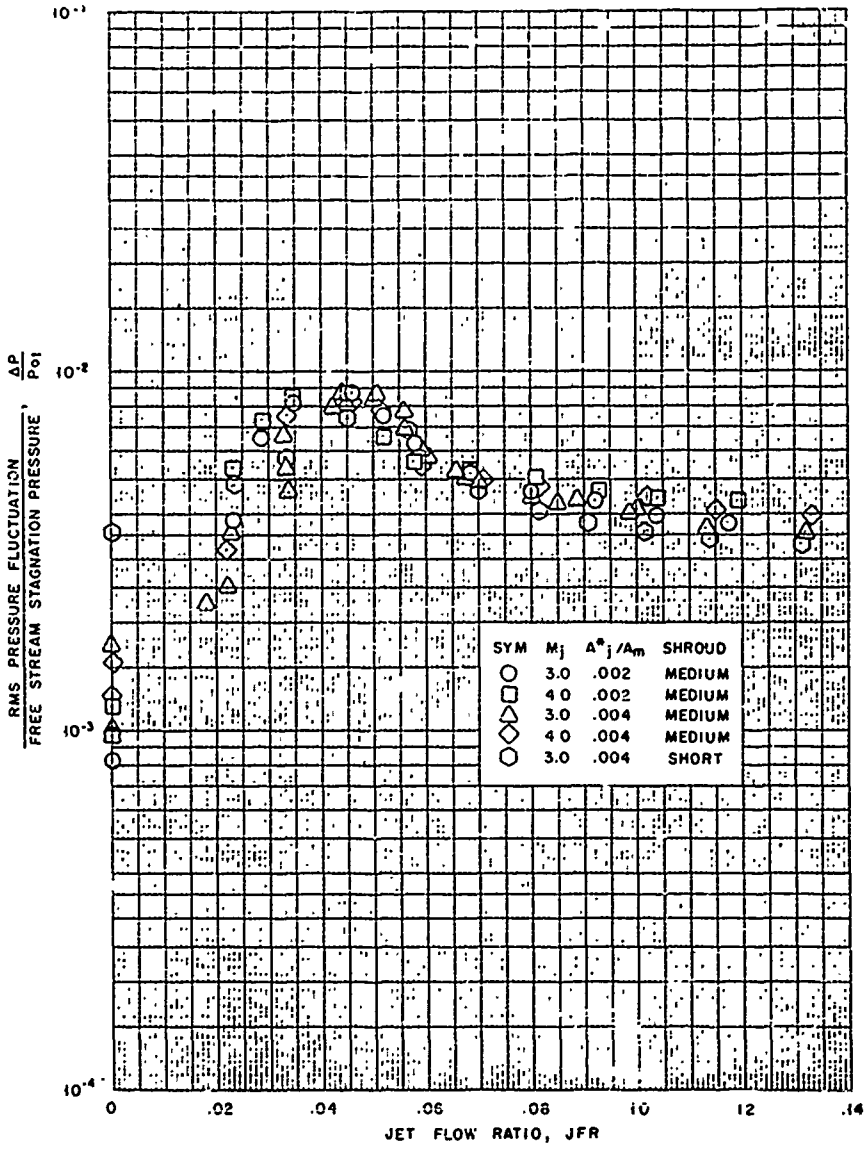

Figure 11. Root Mean Square Internal Pressure Fluctuations vs. Jet Flow Ratio, Jet Parameter Variation

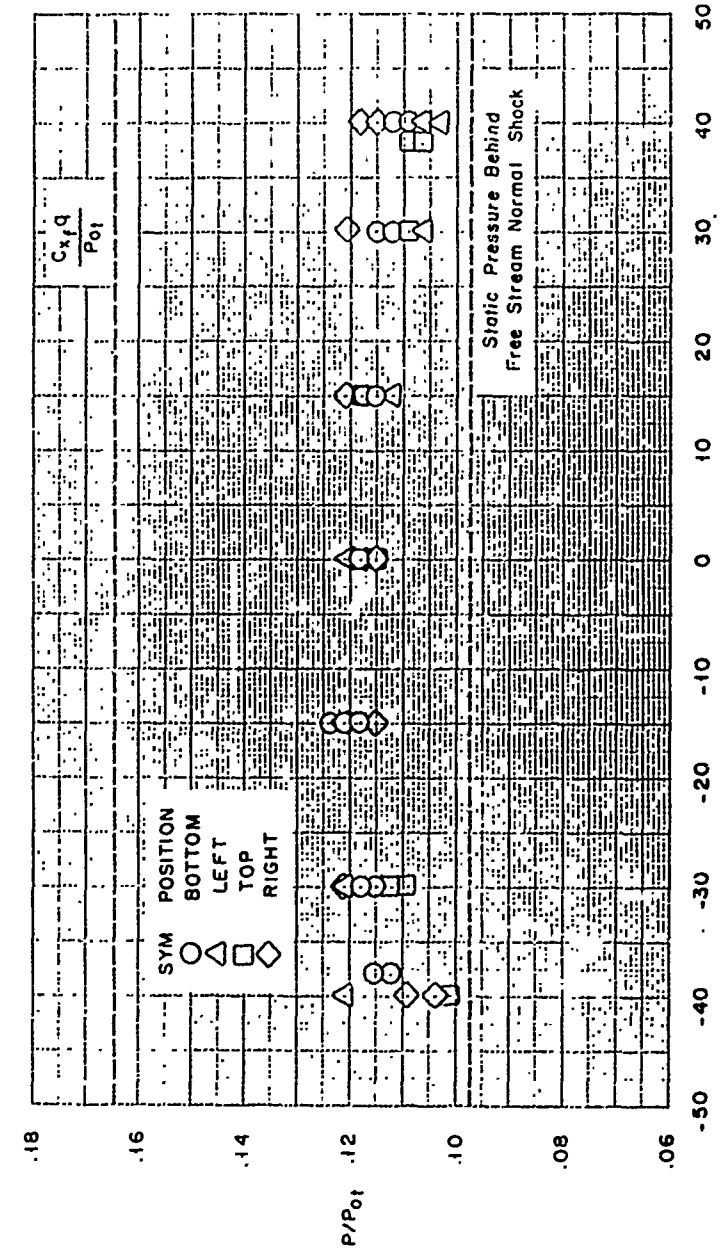

Figure 12. Internal Shroud Pressure as a Function of Telescope Position

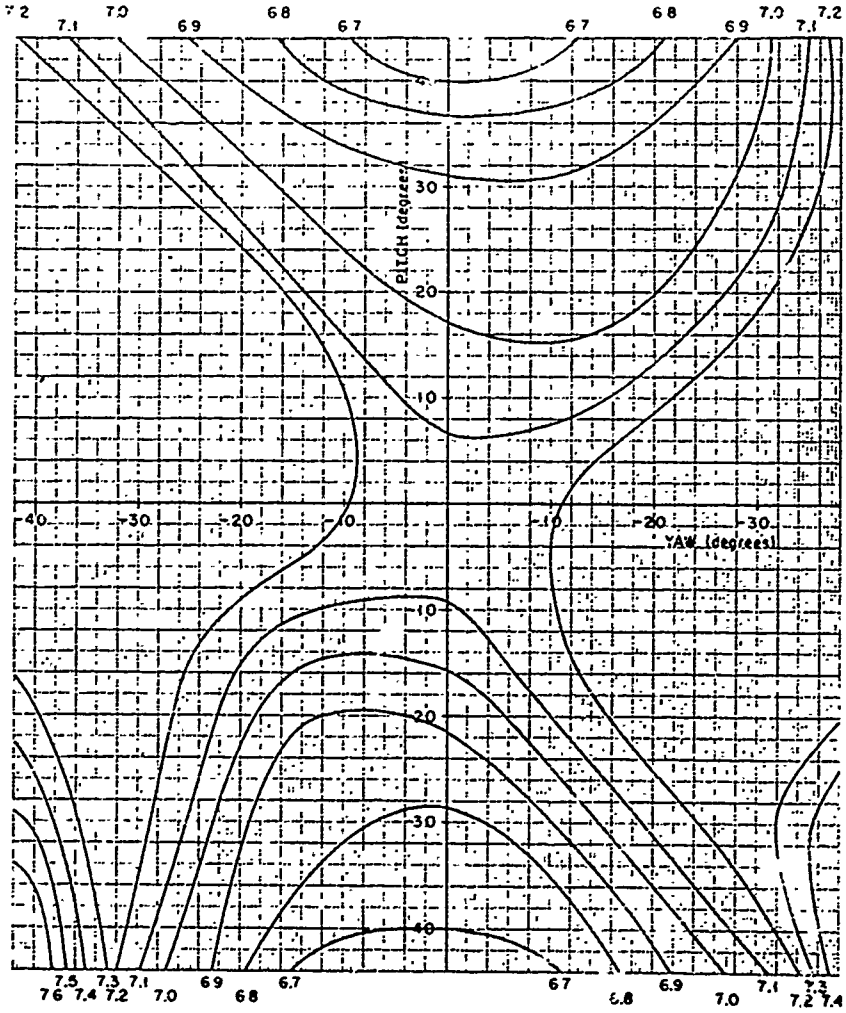

Figure 13. Root Mean Square Internal Pressure Fluctuations as a Function of Telescope Position, Lines of Constant rms $\frac{\Delta P}{P_{0_T}} \times 10^3$

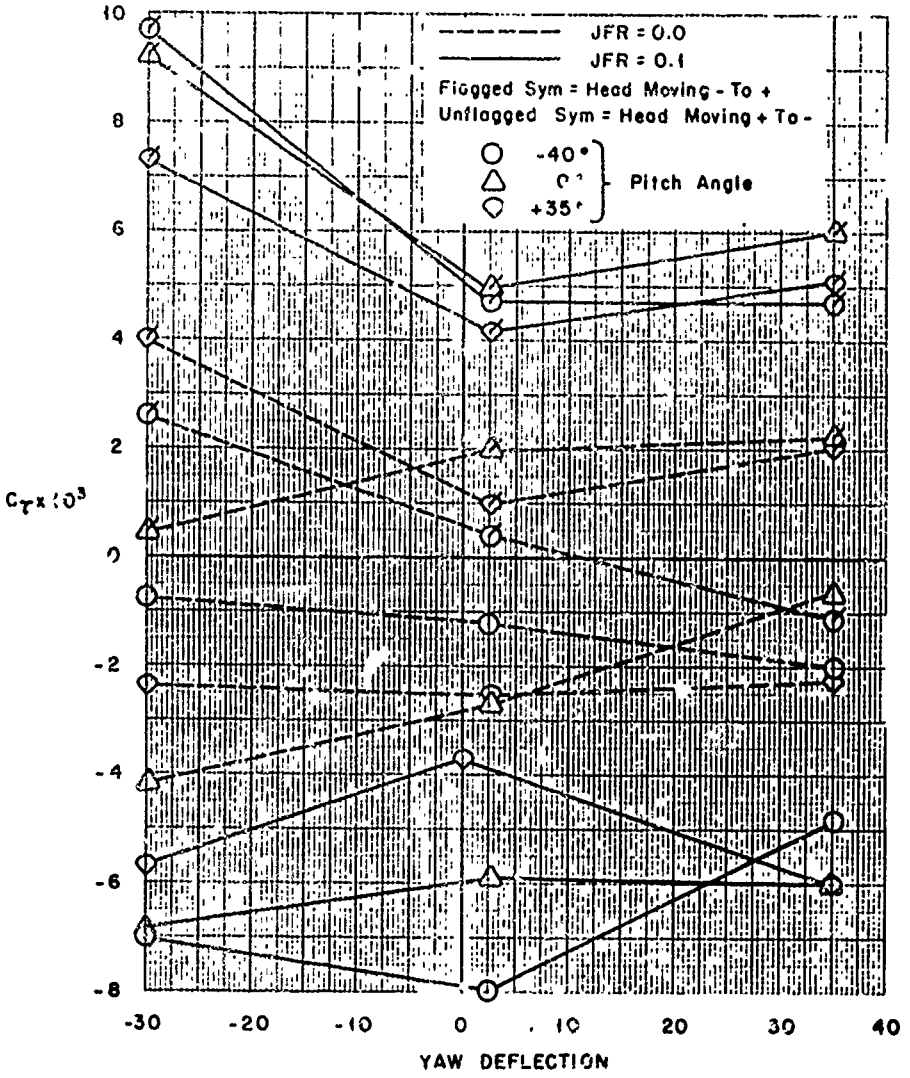

Figure 14. Yaw Torque Coefficient vs. Yaw Deflection, M = 2.75, P_{0_T} = 11.5 psia

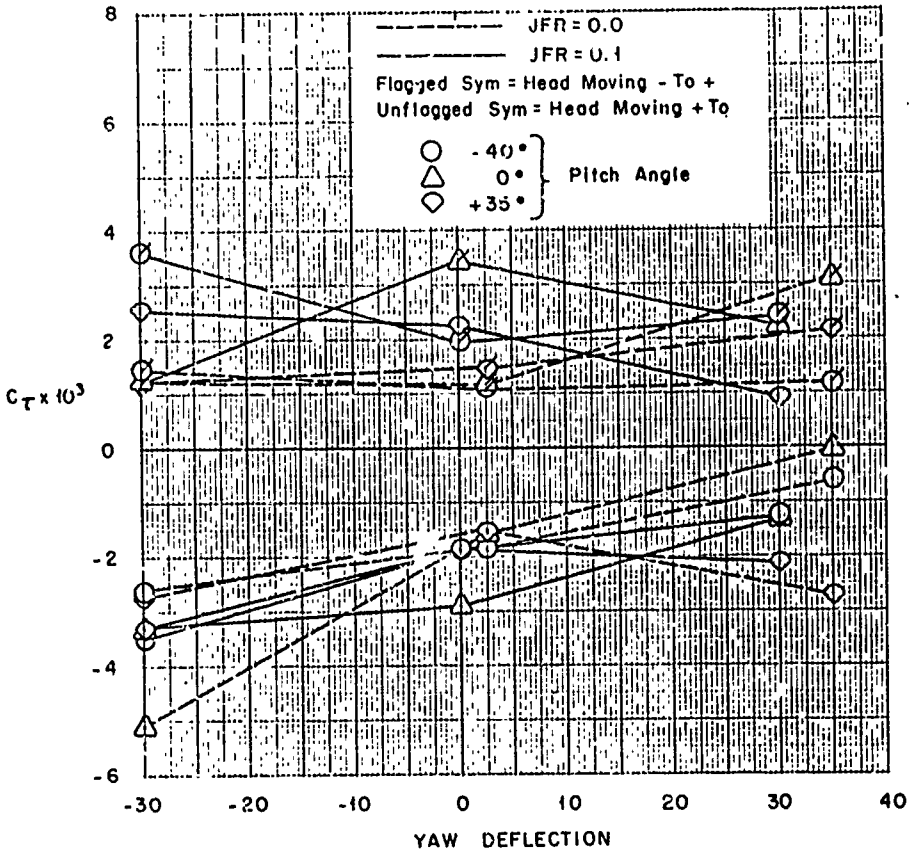

Figure 15. Yaw Torque Coefficient vs Yaw Deflection, M = 2.75, P_{0_T} = 25.0

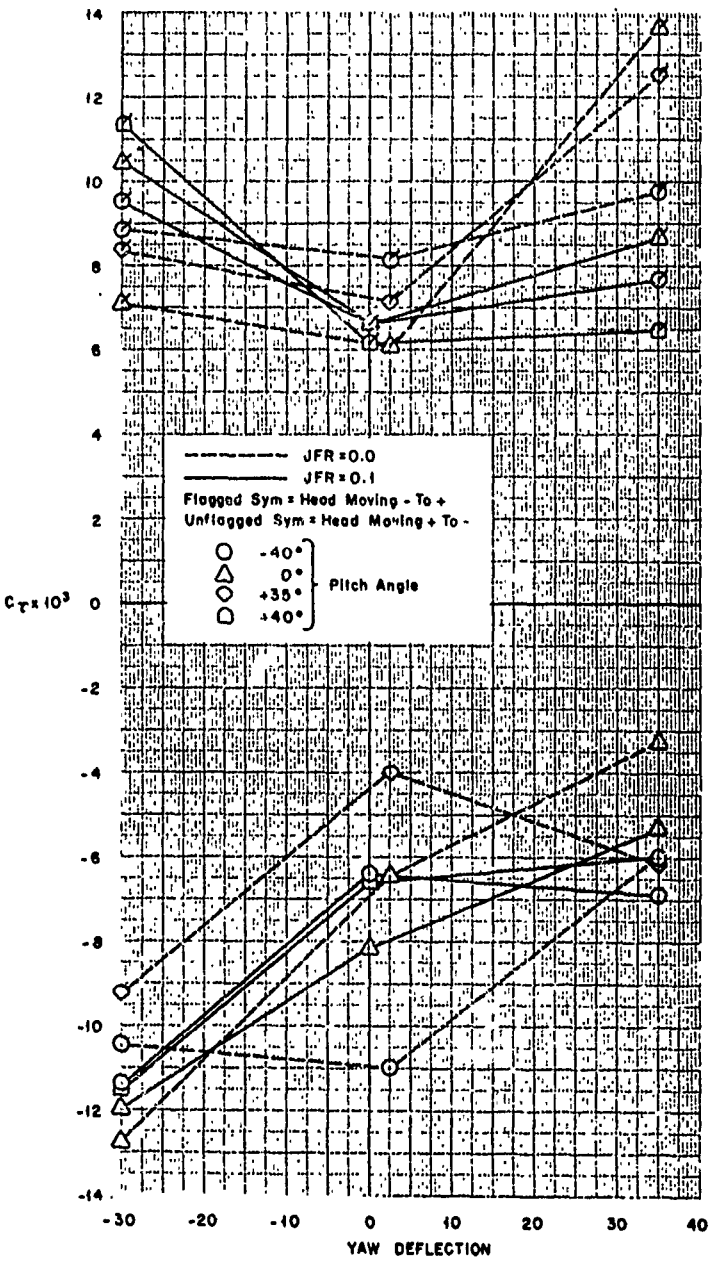

Figure 16. Yaw Torque Coefficient vs. Yaw Deflection, M = 3.00, P_{0_T} = 15.0

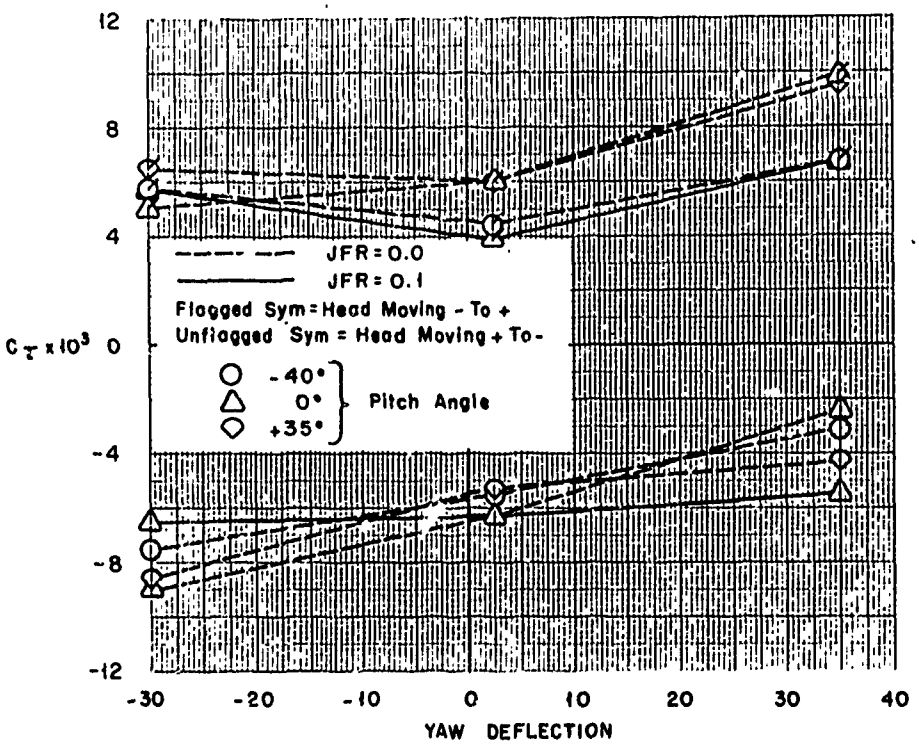

Figure 17. Yaw Torque Coefficient vs. Yaw Deflection, M = 3.00, P_{0_T} = 25.0

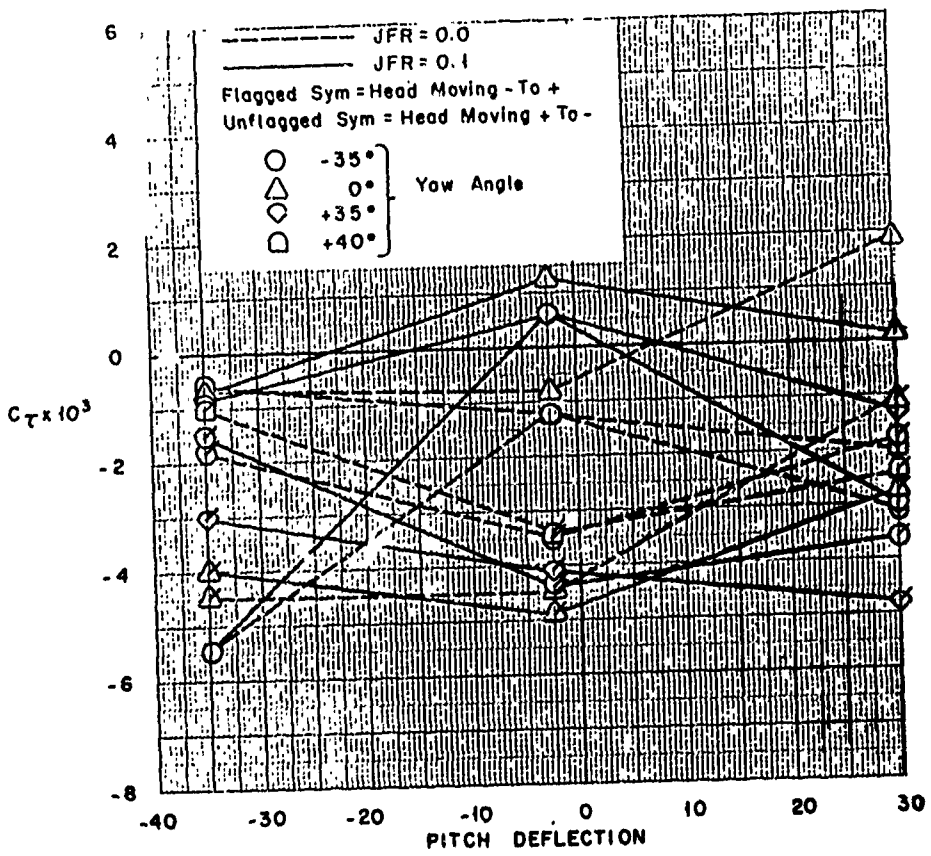

Figure 18. Pitch Torque Coefficient vs. Pitch Deflection, $M = 2.75$, $P_{0_T} = 11.5$

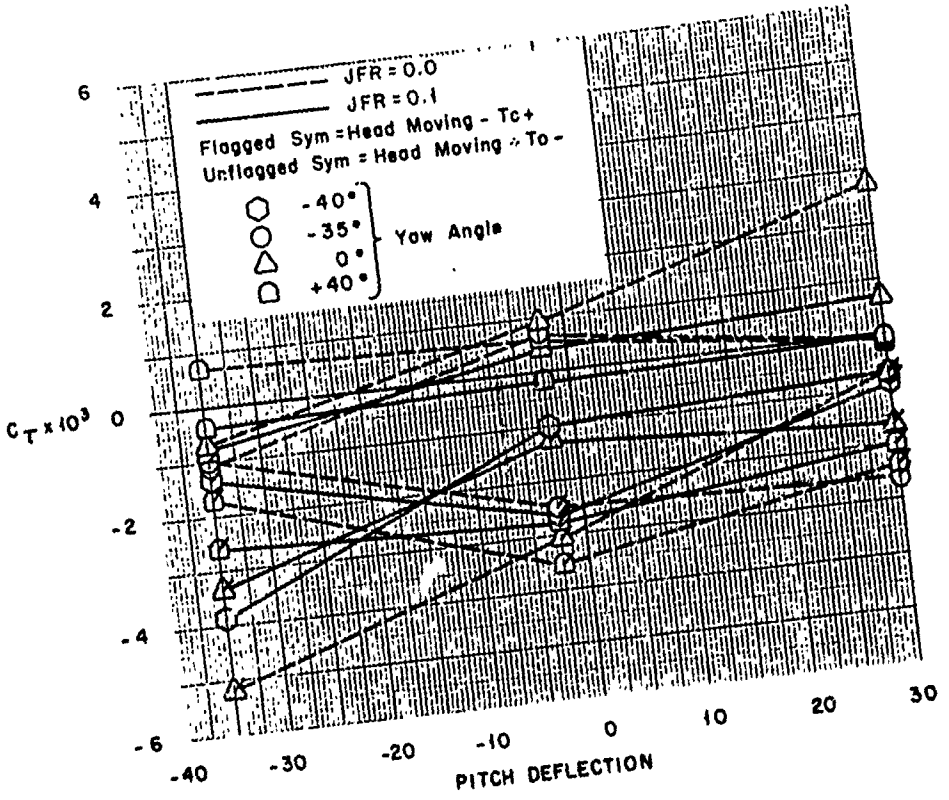

Figure 19. Pitch Torque Coefficient vs. Pitch Deflection, $M = 2.75$, $P_{0_T} = 25.0$

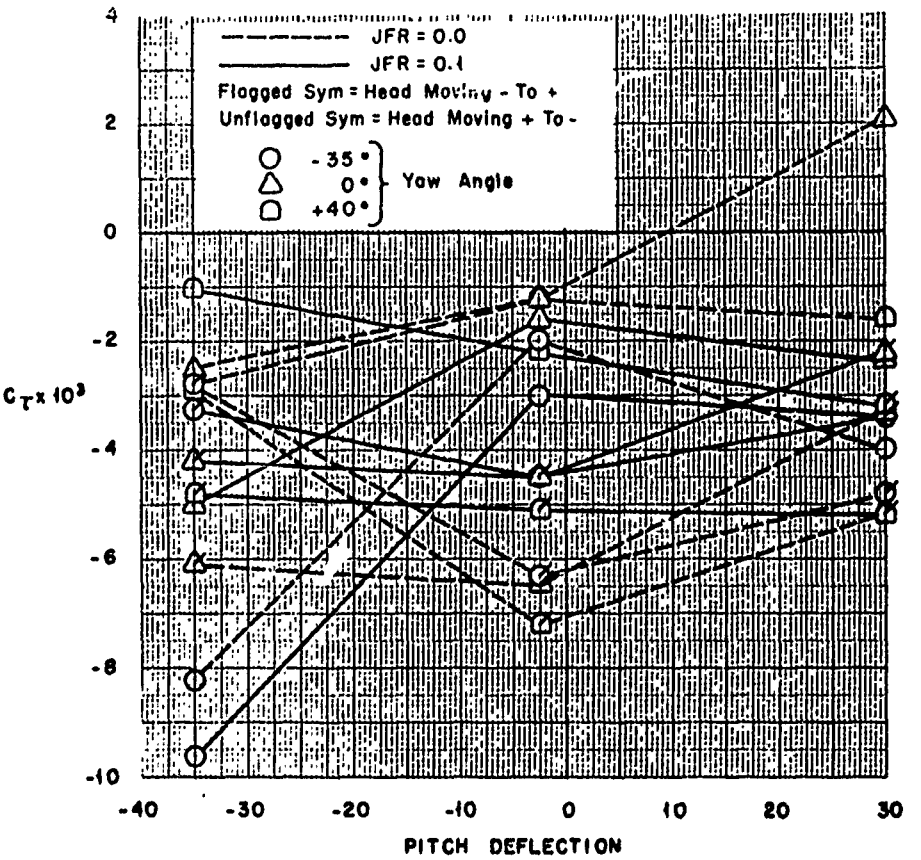

Figure 20. Pitch Torque Coefficient vs. Pitch Deflection, M = 3.00, P_{0_T} = 15.0

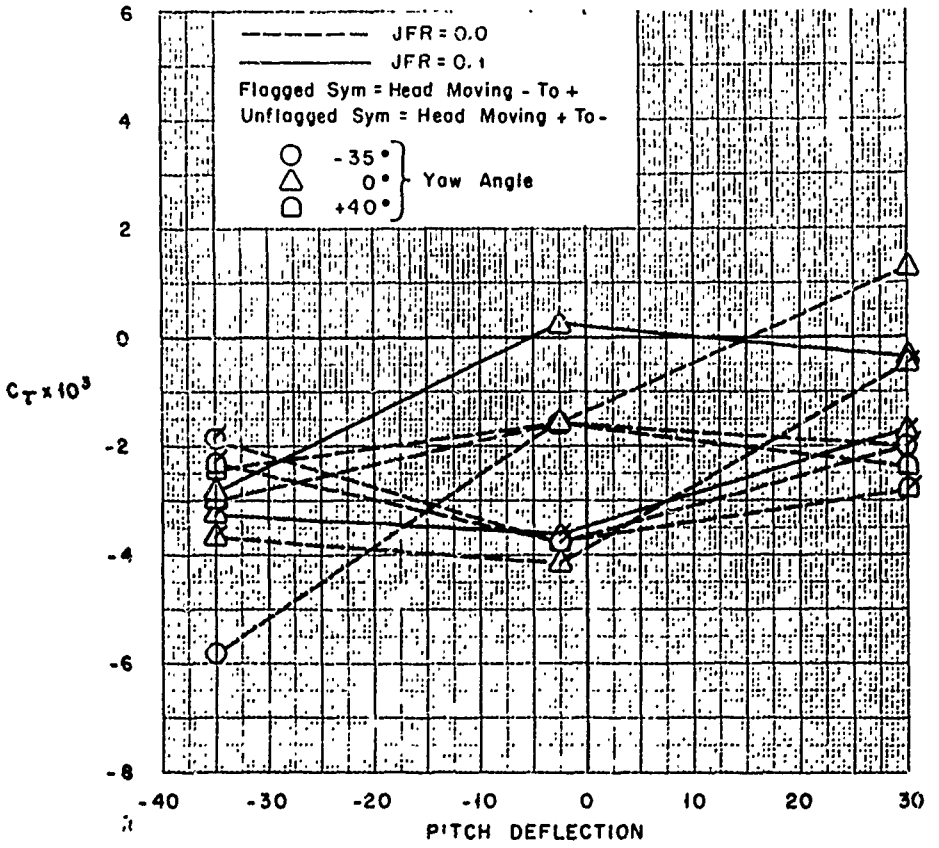

Figure 21. Pitch Torque Coefficient vs. Pitch Deflection, M = 3.00, P_{0_T} = 25.0

APPENDIX
DEVELOPMENT OF AERODYNAMIC WINDOW PARAMETERS

The nose axial force coefficient, C_x, is of primary interest in this program. This is the total force exerted on the nose of the model along its axis divided by the product of the free stream dynamic pressure and model face area. This coefficient is composed of three parts:

$$C_x = \left(\frac{F_x \text{ face pressure}}{qA_m}\right) + \left(\frac{F_x \text{ jet momentum change}}{qA_m}\right) + \left(\frac{F_x \text{ jet exit pressure}}{qA_m}\right)$$

In this case the face area, A_m, is simply the square of the missile radius times pi. The total force due to the face pressure can be found by integrating the pressure over the model face, thus

$$C_{x_f} = \frac{\int P_f dA}{A_m \frac{\gamma}{2} PM^2}$$

In Ref. 4 it was determined that the pressure over the model face is fairly uniform at the minimum drag conditions. Therefore it can be written,

$$C_{x_f} \approx \frac{2(P_f)_{av}}{P\gamma M^2}$$

It is assumed that the momentum of the gas entering the model stilling chamber is negligible, and that there is a nose axial force proportional to the momentum of the jet as it leaves the model. The non-uniformities in flow across the nozzle exit are neglected and the C_x

component due to jet momentum change can be written,

$$C_{x_{jmc}} = \frac{\dot{m}_j V_{jx}}{A_m q} ,$$

or, in terms of known quantities:

$$C_{x_{jmc}} = 2 \sin B \left(\frac{P_{0j}}{P_{0T}}\right) \left(A^*_j/A_m\right) \left(\frac{P_0}{P}\right) \left(\frac{M_j}{M^2_T}\right) \sqrt{\left(\frac{2}{\gamma+1}\right)^{(\gamma+1)/(\gamma-1)} \left(\frac{T}{T_0}\right)_{M_j}}$$

Again, neglecting the non-uniformities across the nozzle exit, a small force due to the pressure at the jet exit can be expressed, in coefficient form, as,

$$C_{x_{ep}} = \frac{1}{\sin B} \left(\frac{P}{P_0}\right)_{M_j} \left(\frac{P_0}{P}\right)_{M_T} \left(\frac{P_{0j}}{P_{0T}}\right) \left(\frac{A_E}{A_m}\right) \frac{2}{\gamma M^2_T}$$

The parameter describing the strength of the jets is the jet flow ratio, JFR, which is the ratio of the mass flow through the jets to the mass flow tnrough a stream tube in the undisturbed free stream with a cross sectional area equal to that of the model face. The jet flow ratio can be written

$$JFR = \left(\frac{A^*_j}{A_m}\right) \left(\frac{P_{0j}}{P_{0T}}\right) \left(\frac{A}{A^*}\right)_{M_T} \sqrt{\frac{T_{0T}}{T_{0j}}}$$

where

$$\frac{A}{A^*} = \left[\frac{216}{125} M \left(1 + \frac{M^2}{5}\right)^{-3}\right]^{-1}$$

for air.